BMC Microbiology

RESEARCH

Open Access

Dual RNA-seq analysis reveals the interaction between multidrug-resistant *Klebsiella pneumoniae* and host in a mouse model of pneumonia

Xiaolin Song[1], Chengyu Sui[1], Meng Lv[1], Cuicui Jiang[2], Lingfei Hu[1], Yongqiang Jiang[1], Dongsheng Zhou[1], Wenhui Yang[1*] and Chenxi Dai[1*]

Abstract

Background Multidrug-resistant *Klebsiella pneumoniae* (MDR-KP) poses a significant global health threat, associated with high morbidity and mortality rates among hospitalized patients. The interaction between MDR-KP and its host is highly complex, and few studies have investigated these interactions from both the pathogen and host perspectives. Here, we explored these interactions in a mouse model of pneumonia using dual RNA-seq analysis.

Methods PCR identification and antimicrobial susceptibility test were employed to screen for MDR-KP strains. A mouse model of pneumonia was established through aerosolized intratracheal inoculation with high-dose or low-dose bacteria. Bacterial loads, pathological changes, inflammatory cytokine expression, and immune cell infiltration were assessed post-challenge. Dual RNA-seq analysis was conducted on lung tissues following infection.

Results NY13307 was identified as an MDR-KP strain with minimal virulence factor genes and broad-spectrum drug resistance. High-dose bacteria induced more severe pulmonary pathological changes, a significant increase in bacterial load, and notably elevated secretion of inflammatory cytokines compared to low-dose bacteria. Alveolar macrophages and resident interstitial macrophages were identified as the primary sources of these cytokines. Further RNA-seq analysis revealed that, compared to the low-dose group, the high-dose group significantly upregulated hypoxia and pro-inflammatory cytokine-related genes in the host, and siderophore-related genes in the bacteria. Correlation analysis demonstrated a significant association between siderophore-related genes and clusters of genes related to pro-inflammatory cytokines and hypoxia.

Conclusions In this mouse model of bacterial pneumonia, excessive siderophore expression may trigger the activation of hypoxia signaling pathways and the release of pro-inflammatory cytokines, ultimately reducing survival rates.

*Correspondence:
Wenhui Yang
fionyoung@163.com
Chenxi Dai
daichenxi@bmi.ac.cn; brycedai0903@163.com

Full list of author information is available at the end of the article

© The Author(s) 2025. **Open Access** This article is licensed under a Creative Commons Attribution-NonCommercial-NoDerivatives 4.0 International License, which permits any non-commercial use, sharing, distribution and reproduction in any medium or format, as long as you give appropriate credit to the original author(s) and the source, provide a link to the Creative Commons licence, and indicate if you modified the licensed material. You do not have permission under this licence to share adapted material derived from this article or parts of it. The images or other third party material in this article are included in the article's Creative Commons licence, unless indicated otherwise in a credit line to the material. If material is not included in the article's Creative Commons licence and your intended use is not permitted by statutory regulation or exceeds the permitted use, you will need to obtain permission directly from the copyright holder. To view a copy of this licence, visit http://creativecommons.org/licenses/by-nc-nd/4.0/.

Keywords Multidrug-resistant *Klebsiella pneumoniae*, Dual RNA-seq analysis, Aerosolized intratracheal inoculation, Hypoxia, Siderophores

Introduction

Klebsiella pneumoniae (*K. pneumoniae*), one of the most common gram-negative opportunistic pathogens, is a leading cause of hospital-acquired pneumonia, particularly in developing countries, where it accounts for up to 10% of all nosocomial infections [1, 2]. It can cause pneumonia, urinary tract infections, meningitis, bacteremia, and other diseases in individuals with compromised immune systems or those frequently exposed to healthcare settings, such as neonates, the elderly, and intensive care unit patients. Due to the misuse of antibiotics, *K. pneumoniae* has evolved towards multidrug resistance, and its high level of resistance has landed it on the World Health Organization's list of priority concerns [3]. Carbapenem-resistant *K. pneumoniae*, which produces broad-spectrum beta-lactamases and is resistant to carbapenems, causes over 90,000 infections and more than 7,000 deaths annually in Europe [4]. Additionally, *K. pneumoniae* strains that are multidrug-resistant to third-generation cephalosporins, fluoroquinolones, carbapenems, and aminoglycosides have also greatly emerged [5]. The infections caused by *K. pneumoniae* are gradually becoming uncontrollable by modern medicine, making it urgent to explore the mechanisms of interaction between *K. pneumoniae* and the host after infection and to seek alternative therapies.

The interaction between *K. pneumoniae* and its host is extremely intricate. Lung et al. combined in situ metabolic imaging and transcriptional analyses to demonstrate that *K. pneumoniae* activates host glutaminolysis and fatty acid oxidation, and then they concluded that *K. pneumoniae* induces host metabolic stress that promotes tolerance to pulmonary infection [6]. Our previous study conducted a time-course transcriptome analysis of lungs from mice infected with hypervirulent *K. pneumoniae* via aerosolized intratracheal inoculation, and found that it causes primary acute inflammation in the lung that intensifies over time, leading to the destruction of lung tissue [7]. Mackel et al. highlighted the protective role of lung macrophages, especially interstitial macrophages, following *K. pneumoniae* infection through depletion experiments [8]. Despite numerous studies dedicated to understanding the pathogenic mechanisms of *K. pneumoniae*, few have investigated the interaction mechanisms from the perspective of both the pathogen and host at the transcriptional level. Dual RNA-seq, first reported in 2012 [9], enables the simultaneous sequencing and analysis of gene expression in both the pathogen and host, aiding in the more precise revelation of gene expression dynamics during their interaction. However, to date, only one cellular experimental study has utilized dual RNA sequencing to analyze the interplay between *K. pneumoniae* and human lung epithelial cells, emphasizing the importance of the OmpR regulon as a promising target for anti-virulence drug discovery programs [10]. Thus, it is urgent for us to deeply investigate the interactions of *K. pneumoniae* and host by using dual RNA-seq.

In this study, we meticulously selected a multi-drug-resistant *K. pneumoniae* (MDR-KP) strain NY13307 through a rigorous process that began with PCR identification and antimicrobial susceptibility test on 18 clinical isolates, aiming to identify strains with minimal virulence genes and a broad spectrum of drug resistance. Following this, we confirmed the virulence of the strains in vivo using an aerosolized intratracheal inoculation model in mice, ultimately selecting the NY13307 strain for its low virulence profile and multi-drug resistance attribute. We then proceeded to assign mice to receive either high or low doses of *K. pneumoniae*, monitoring bacterial loads, pathological changes, flow cytometry analysis, and the expression levels of pro-inflammatory cytokines in bronchoalveolar lavage fluid (BALF). Finally, we employed dual RNA-seq analysis on lung tissues from infected mice to verify the observed biological phenomena and to delve into the pathogenic mechanisms of *K. pneumoniae*, by comparing the host and pathogen gene transcriptome profiles across two distinct disease endpoint models.

Materials and methods

Animals and ethics statement

Specific pathogen-free, female C57BL/6J mice (6 to 8 weeks old, 18–20 g) were obtained from HFK Bio-Technology Co., Ltd. (Beijing, China). All procedures involving these experimental animals were carried out within the Animal Biosafety Level-2 (ABSL-2) laboratory. This study was approved by Institute Animal Care and Use Committee of Academy of Military Medical Sciences with the ethical approval number of IACUC-DWZX-2024-007.

Bacterial strain and growth

All 18 *K. pneumoniae* strains in this study were clinical isolates. The NY13307 strain (CP109963, ST11/CG258) was isolated from a sputum sample of a hospitalized patient in Beijing, China. The strain was inoculated in brain heart infusion (BHI) broth (BD Biosciences, Lawrence, KS) at a ratio of 1:1000 and incubated in a shaker at 37 ℃, 200 rpm overnight, providing the first generation of culture in the stationary stage. Subsequently, the culture was diluted at 1:250 with BHI and maintained at 37 ℃ for 2.5 h, which was the second-generation culture

at the middle logarithmic phase. Then, the culture was further diluted and incubated for another 3 h to reach OD600 = 1.5. After that, the culture was adjusted to OD600 = 1.0 for subsequent use, with a concentration of approximately 4×10^8 CFU/mL. Meanwhile, the inoculation dose was also determined by serial dilution plating on BHI agar for each experimental trial.

Polymerase chain reaction (PCR) identification

The species-specific gene, virulence genes, and virulence plasmids of 18 strains were detected by PCR. Briefly, the reaction mixture (30 μL) consisted of 3 μL template DNA, 15 μL 2x Taq PCR Master Mix (MT201, Biomed, China), 0.3 μL of each forward and reverse primers, and 11.4 μL ddH_2O. Primer sequences were listed in Table S1. A reaction mixture without template DNA was used as a negative control. The PCR reaction conditions were optimized as follows: a pre-denaturation step at 95 °C for 5 min, followed by 30 cycles of denaturation at 95 °C for 30 s, annealing at each primer's specific annealing temperature for 30 s, and extension at 72 °C for 30 s. After the cycles, a final extension was performed at 72 °C for 10 min, and the samples were then held at 4 °C. The PCR products were subjected to electrophoresis on a 1.5% agarose gel stained with TS-gelred, and the results were imaged using UV light with the iBringht 750 device.

Antimicrobial susceptibility test

Antimicrobial susceptibility testing was performed using the broth microdilution method in strict accordance with the Clinical and Laboratory Standards Institute (CLSI) guidelines. The minimum inhibitory concentration (MIC) was determined for the following antimicrobial agents: ampicillin, piperacillin, cefazolin, cefuroxime, meropenem, amikacin, levofloxacin, trimethoprim/sulfamethoxazole, and tigecycline. MIC values were interpreted using CLSI-recommended breakpoints: isolates were classified as susceptible (S) if the MIC was below the susceptibility breakpoint, resistant (R) if the MIC met or exceeded the resistance breakpoint, and intermediate (I) if the MIC fell between the susceptible and resistant thresholds. Multi-drug resistance (MDR) was defined as resistant to three or more classes of antibiotics.

Bacterial challenge

To compare the virulence of NY13294 and NY13307, mice were challenged with bacteria via aerosolized intratracheal inoculation, as described previously [11], with the inoculation dose ranging from 1×10^4 CFU to 1×10^{10} CFU. Each group consisted of 10 mice. After challenge, mice were observed every 24 h, and the survival status was recorded for LD_{50} calculation.

In order to construct a *K. pneumoniae* pulmonary infection model with NY13307 strain, mice were challenged with two specific doses: 3×10^8 CFU for the high-dose group, designed to create a lethal infection model, and 7×10^6 CFU for the low-dose group, aimed at establishing a sub-lethal infection model.

Sample collection

At the indicated time points post-challenge, mice were euthanized by intraperitoneal injection of 200 mg/kg sodium pentobarbital. Lung tissues were then collected for determination of bacterial load, pathological examination, flow cytometry experiments, and RNA extraction. BALF was obtained by inserting a sterile cannula into the trachea and instilling 1 mL of sterile saline, which was subsequently used for cytokine detection.

Determination of bacterial load

At 0, 6, 12, 18, and 24 h after challenge, lungs were harvested from three mice in each group. Then, the lung tissue homogenates were serially diluted and subsequently plated on blood agar plates, followed by incubation at 37 °C overnight. The number of bacterial colonies was determined by counting the colonies that formed.

Pathological examination

At 0,6,12,18, and 24 h after challenge, lungs were harvested from three mice in each group. The lungs were immersed in the tissue fixative solution for 24 h. After soaking, lung tissue was dehydrated, paraffin-embedded, and sectioned. Prior to evaluation, sectioned tissues were stained with hematoxylin and eosin. The degree of pathological changes, such as hemorrhage, degeneration, necrosis, and inflammatory changes, were evaluated in the tissue sections, as described previously [12].

Cytokines expression

Levels of pro-inflammatory cytokines were measured using cytometric bead array (CBA), according to the manufacturer's protocol. Briefly, BALF were incubated with capture and detection beads for a selected panel of cytokines IL-1β, IL-6, IL-17 A, IL-12p70, TNF-α, and GM-CSF. Samples were measured on an LSRFortessa (BD Biosciences) and analyzed using FlowJo (version 10.4.1, Treestar).

Immune cells measurement using flow cytometry

To better understand the pathogenetic mechanisms in mice after high-dose and low-dose challenges, we used flow cytometry to measure immune cell number and status at the indicated time points. Lung tissues were collected and single-cell suspensions were obtained through digestion and removal of red blood cells using red blood cell lysis buffer. Subsequently, the single-cell suspensions were incubated with FVD780 dye (Sigma-Aldrich) at room temperature for 10 min, followed by incubation

with the indicated antibodies on ice for 30 min: CD45 (BUV395, BD Biosciences, 564279), Ly6G (Percp-Cy5.5, BD Biosciences, 560602), CD11c (BV786, BD Biosciences, 563735), CD11b (BV605, Biolegend, 101237), Ly6C (PE-Cy7, BD Biosciences, 569442), SiglecF (AF647, BD Biosciences, 562680), F4/80 (BV421, BD Biosciences, 565411), CD80 (FITC, BD Biosciences, 561954), CD3 (BV510, BD Biosciences, 563024), CD19 (BV711, Biolegend, 115555). After staining, cells were washed and resuspended in DPBS. Samples were acquired using a FACS LSRFortessa (BD) and analyzed with FlowJo (version 10.4.1, Treestar).

RNA extraction, library preparation, and sequencing

At indicated time points post-challenge, lung tissues were harvested. Total RNA was extracted using TRIzol reagent, followed by digestion with DNaseI. The quality of RNA was determined by measuring the A260/A280 ratio with a spectrophotometer. RNA integrity was confirmed using an automated nucleic acid and protein analysis system. Qualified RNA was ultimately quantified using Qubit™ RNA High Sensitivity (HS), Broad Range (BR), and Extended Range (XR) Assay Kits. Library construction and sequencing were performed for qualified RNA samples at Wuhan Kangce Technology Co., Ltd. For library preparation, the RNA of each sample was used for stranded dual RNA sequencing library preparation using Ribo-off rRNA Depletion Kit (Vazyme, China, cat. #N406 for animal, cat. #N407 for bacteria) to deplete rRNA, and then components of KCTM Digital Stranded mRNA Library Prep Kit (Seqhealth Tech. Co., Ltd. Wuhan, China) following the manufacturer's instruction. The kit eliminates duplication bias and errors in PCR and sequencing steps, by using unique molecular identifier (UID) of 12 random bases to label the pre-amplified cDNA molecules.PCR products corresponding to fragments ranging from 200 to 500 base pairs were enriched, quantified and sequenced on a DNBSEQ-T7 platform using the PE150 mode to generate paired-end reads. Raw sequencing data was first filtered by fastp (version 0.23.0), low-quality reads were discarded and the reads contaminated with adaptor sequences were trimmed. Clean reads were further treated with in-house scripts to eliminate duplication bias introduced in library preparation and sequencing.

The reference genomes of the two species were merged, and then the deduplicated data were mapped to the two reference genomes of Mus musculus from ftp://ftp.ensembl.org/pub/release-87/fasta/mus_musculus/dna/ and *K. pneumoniae* from https://www.ncbi.nlm.nih.gov/nuccore/CP109963 using STAR software (version 2.5.3a) with default parameters. The reads mapped to the exon regions of each gene were counted by featureCounts (Subread-1.5.1; Bioconductor).

Dual RNA-seq analysis

RNA-seq data were analyzed using R (R version 4.1.0). The EdgeR package was utilized to identify differentially expressed genes (DEGs) [13]. The selection criteria for identifying DEGs were an adjusted P value < 0.05 and a|log2 Fold Change| >1. To analyze the DEGs and gene sets, we employed the Bioconductor package clusterProfiler [14], which offers Gene Ontology and pathway-enrichment analysis using the Kyoto Encyclopedia of Genes and Genomes database. We also applied the Mfuzz R package to perform cluster analysis on the gene dynamic expression patterns, which was based on a fuzzy C-means algorithm with a cluster number of 6 and a fuzzy coefficient M of 2 [15].

Statistical analysis

All statistical analyses were performed using GraphPad Prism version 8. Bacterial loads, histopathological scores, and cytokine concentrations were assayed by two-way analysis of variance (ANOVA). One-way analysis of variance or repeated measures of two-way analysis of variance and post-hoc multiple comparison tests were used for normally distributed variables. Survival analysis was conducted using the Kaplan-Meier method and the log-rank test. Spearman correlation analysis was conducted to measure the correlation of host and bacterial genes. A $P < 0.05$ was considered statistically significant.

Results

Establishing lethal and sub-lethal models of pneumonia

We employed the process outlined in Fig. 1a to screen for MDR-KP strains, ultimately selecting the NY13307 strain. Initially, we conducted a PCR identification of species-specific genes, virulence genes, and the main virulence plasmids for 18 clinical isolates (Figure S1). The screening criteria for PCR were as follows: (1) the strain contained the *K. pneumoniae* species-specific gene *khe*, lacked the high-virulence genes *peg-344* and *iucA* [16], and possessed only one main virulence plasmid, (2) it harbored as few virulence genes as possible to increase the challenge dose for the animal model. Based on these criteria, we identified three strains NY10906, NY13294, and NY13307. Considering the MDR characteristics of *K. pneumoniae* in clinical settings, our goal was to obtain a strain with such properties. We conducted an antimicrobial susceptibility test on 18 clinical isolates, which included nine antibiotics covering seven classes of antibiotics to which *K. pneumoniae* is prone to develop resistance, such as carbapenems, penicillins, and cephalosporins (Table S2). The findings indicated that strain NY10906 exhibited resistance to only one class of antibiotics, whereas strains NY13294 and NY13307 demonstrated resistance to four classes of antibiotics. Therefore, these two strains were selected for in vivo virulence

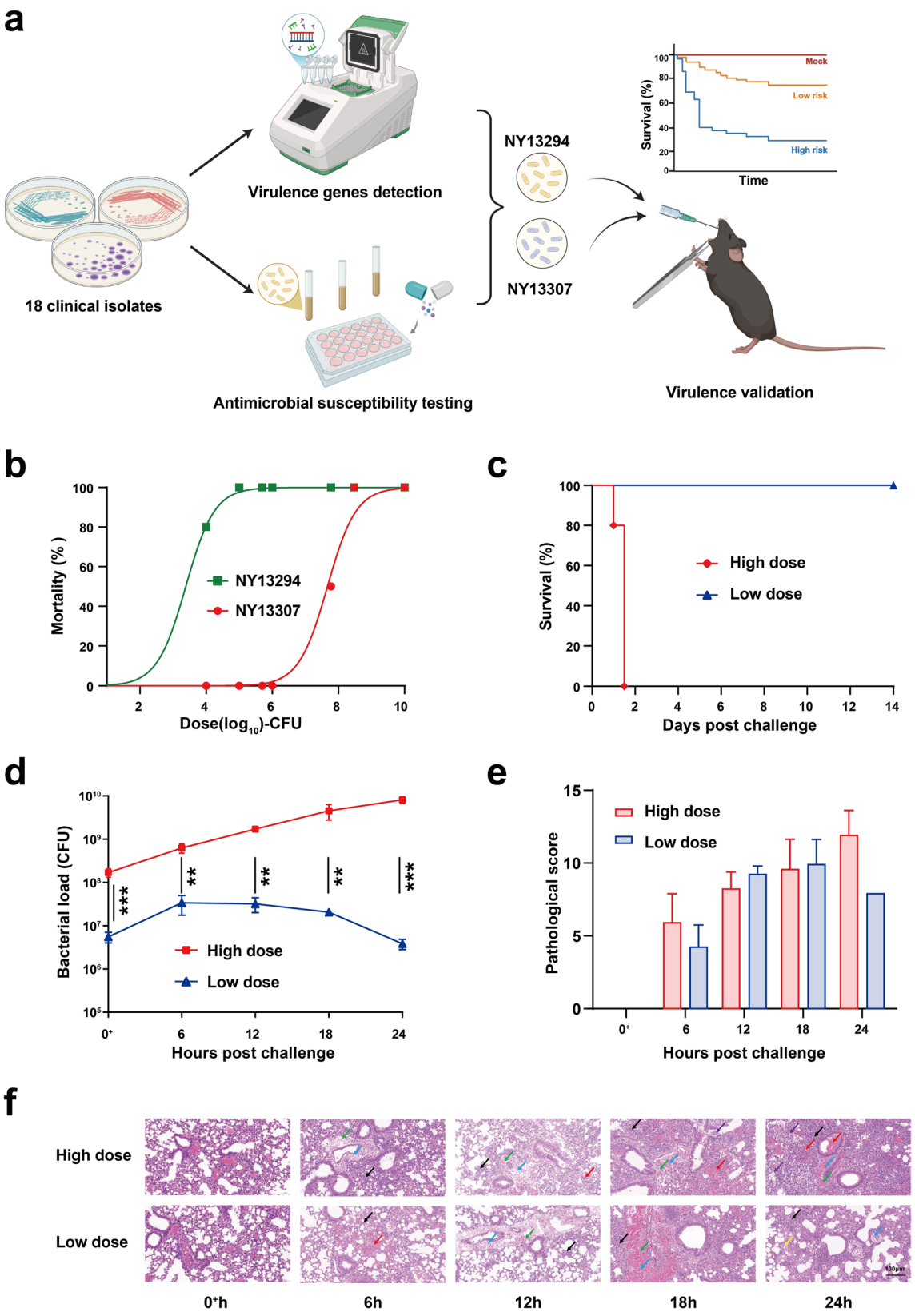

Fig. 1 Establishing lethal and sub-lethal mouse model of *K. pneumoniae* infection. **a**, Schematic diagram of the strain selection process. **b**, Comparison of virulence between NY13294 and NY13307. **c**, Survival curves after high-dose and low-dose challenges. **d**, Bacterial load in the lungs after challenge. **e**, Pathological scores of lung tissue. **f**, Pathological sections of lung tissue

validation. Using different doses for aerosol pulmonary delivery challenge in mice, the LD_{50} for strain NY13294 was 2×10^3 CFU, while for strain NY13307, the LD_{50} was 5×10^7 CFU (Fig. 1b). According to the previous study [17], bacterial loads above 2×10^6 CFU are more conducive to dual transcriptomics analysis. Given that NY13307 has a larger LD_{50}, indicating a higher bacterial colonization in the lungs, this strain was chosen for the following study.

Subsequently, we further determined lethal dose and sub-lethal dose for the NY13307 strain in mice, which were 3×10^8 CFU and 7×10^6 CFU, respectively, designated as the high-dose and low-dose groups (Fig. 1c). Bacterial loads in the lungs of mice at various time points after challenge were measured. In the high-dose group, the bacterial load in the lungs showed an increasing trend within 24 h post-challenge, leading to a high mortality rate, consistent with the characteristics of acute infection. For the low-dose group, bacteria load initially increased, reaching a peak of 3×10^7 CFU at 6 h post-challenge, then it progressively declined, and by 24 h post-challenge, it returned to the level at 0 h (Fig. 1d). Pathological examination of lung tissue revealed that the high-dose group began to exhibit thickening of alveolar walls and inflammatory cell infiltration at 6 h post-challenge, with the lesions progressively worsening. At 24 h post-challenge, the lung tissue showed significant hemorrhage and structural destruction. The low-dose group began to show small areas of alveolar wall thickening accompanied by a few neutrophil infiltrations at 6 h, and as the disease progressed, the lesions intensified at 12 and 18 h and then alleviated at 24 h (Fig. 1e-f).

High-dose infection induced significantly increased pro-inflammatory cytokines than low-dose infection

We examined the concentrations of various cytokines in BALF at various time points post-challenge (Fig. 2). For the high-dose group, the concentrations of six cytokines continued to rise after infection and remained at relatively high levels, including the pro-inflammatory factors IL-1β, IL-6, IL-17 A, IL-12p70, TNF-α, and GM-CSF. These cytokines have all been confirmed to be associated with *K. pneumoniae* infection [18–21], and their combined action may lead to exacerbated inflammation, ultimately resulting in acute pneumonia and death in mice. In contrast, the cytokine concentrations in the low-dose group were significantly reduced compared to the high-dose group. IL-1β remained at a low level after infection,

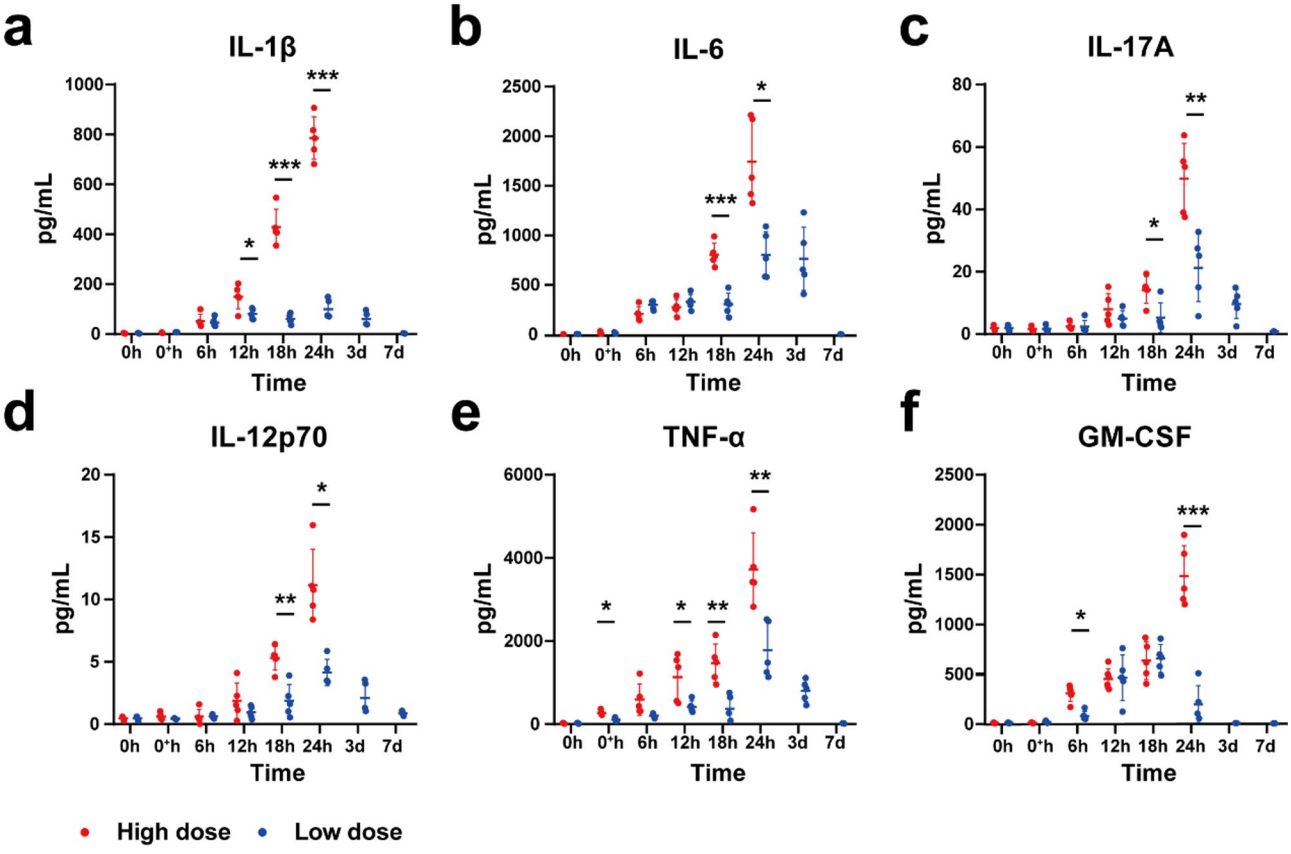

Fig. 2 Cytokine levels in the bronchoalveolar lavage fluid after challenge. **a**, IL-1β. **b**, IL-6. **c**, IL-17 A. **d**, IL-12p70. **e**, TNF-α. **f**, GM-CSF. *: $P<0.05$, **: $P<0.01$, ***: $P<0.001$

while IL-6, IL-17 A, IL-12p70, and TNF-α peaked at 24 h and then declined as the infection gradually cleared, returning to normal levels by 7 d.

Macrophage secreted remarkably elevated pro-inflammatory cytokines

We next utilized flow cytometry to precisely analyze the immune cell response following high-dose and low-dose MDR-KP infection (see gating strategy in Figure S2). Initially, we specifically labeled lung phagocytes by aerosolized intratracheal inoculation of fluorescent PKH26-PCL dye 24 h prior to infection [12]. Neutrophils ($Ly6G^+$), monocytes ($Ly6C^+$), alveolar macrophages (AM, $F4/80^+$ $CD11b^+$), and interstitial macrophages (IM, $F4/80^+$ $SiglecF^+$ $CD11c^+$) were rapidly recruited following infection (Fig. 3a). Unlike neutrophils and monocytes, which continued to increase after infection, the number of macrophages, including AM and IM, decreased from 0 h to 24 h post-infection. Surprisingly, no significant differences were observed between the high-dose and low-dose groups in terms of these cell numbers at each time point. Due to the death of animals in the high-dose group, we only observed a lower number of neutrophils and a higher number of monocytes and macrophages at 168 h post-infection compared to 24 h in the low-dose group, indicating recovery from the infection.

We selected TNF-α as the representative pro-inflammatory cytokine and measured its expression in these cells at 24 h post-infection, as the differences in pro-inflammatory cytokines between the two groups were most pronounced at this time point. The high-dose group exhibited significantly increased TNF-α expression from neutrophils, monocytes, AM, and IM compared to healthy animals, while the low-dose group only showed markedly elevated TNF-α expression from monocytes and IM compared to the mock group (Fig. 3b). We then tracked the resident ($PKH26^+$) and recruited ($PKH26^-$) macrophages throughout the infection at 24 h post-infection (Fig. 3c). We found that both resident and recruited AM expressed significantly higher levels of TNF-α in the high-dose group compared to healthy animals and those treated with the low-dose bacteria, while this phenomenon was not observed in the low-dose group. Additionally, $PKH26^+$ IM exhibited notably higher TNF-α expression in the high-dose group compared to the low-dose and mock groups (Fig. 3d). To determine whether the high-level TNF-α expression originated from classically activated macrophages (M1), we measured CD80 expression in AM and IM. We observed significantly elevated CD80 expression in AM, PKH26 + AM, PKH26- AM, IM, PKH26 + IM, and PKH26- IM (Fig. 3e). However, no differences were observed between the high-dose and low-dose groups in either resident or recruited macrophages (Fig. 3e).

Hypoxia and high-level pro-inflammatory cytokine expression were associated with survival revealed by host RNA-seq

To explore transcriptional changes, we collected and sequenced RNA from mouse lungs before and after infection with *K. pneumoniae* with high-dose or low-dose. Initially, we examined the gene expression dynamics in the host and utilized principal component analysis (PCA) to evaluate the data quality and sample distribution, as depicted in Fig. 4a. Our analysis indicated that the first principal component (PC1) accounted for 72.30% of the total variance in gene expression, while the second principal component (PC2) explained 16.06%. The high reproducibility observed among replicate samples from the same time points and groups highlighted the reliability of our experimental protocols. However, samples collected at different time points and from different groups exhibited distinct transcriptional signatures, suggesting both temporal shifts and dose-dependent effects in gene expression profiles throughout the infection process. Compared to the low-dose group, our analysis revealed the following numbers of differentially expressed genes (DEGs) at the specified time points: 170 at 0 h, 954 at 6 h, 3485 at 12 h, 3459 at 18 h, and 5603 at 24 h (Fig. 4b). Specifically, the number of upregulated DEGs at 0, 6, 12, 18, and 24 h were 124, 480, 1790, 1362, and 2142, respectively, while the counts of downregulated DEGs at these time points were 46, 474, 1695, 2097, and 3461, respectively.

It was noted that the upregulated and downregulated DEGs across different time points showed varying levels of intersection. The volcano plots for each time point, depicted in Fig. 4c, demonstrated that the absolute values of the log2 fold change for DEGs increased over time, indicating a pronounced transcriptional response. The corresponding genes of above six pro-inflammatory cytokines including IL-1β, IL-6, IL-17 A, IL-12p70, TNF-α and GM-CSF showed the same tendence as the expression of these cytokines (Fig. 2, Figure S3), indicating the consistency between the two types of data. Additionally, we identified several meaningful up-regulated DEGs related to pro-inflammatory cytokines or chemokines, such as IL-1α, KC, G-CSF, CCL-2, and MIP-2, as well as hypoxia markers, including HIF-1α, PHD2, PHD3, VHL, PGK1, PKM, and LDHA (Fig. 4c, and Figure S3).

We then performed GO and KEGG analyses to evaluate the functional processes at each time point. GO analysis revealed up-regulated DEGs were associated with innate immune cells (myeloid leukocyte activation, macrophage migration, neutrophil mediated cytotoxicity), cytokine production (IL-1β production, IL-6 production, IL-12 production, IL-17 production, TNF production) and signal pathway activation (canonical NFκB signal transduction, TLR signal pathway) (Fig. 4d).

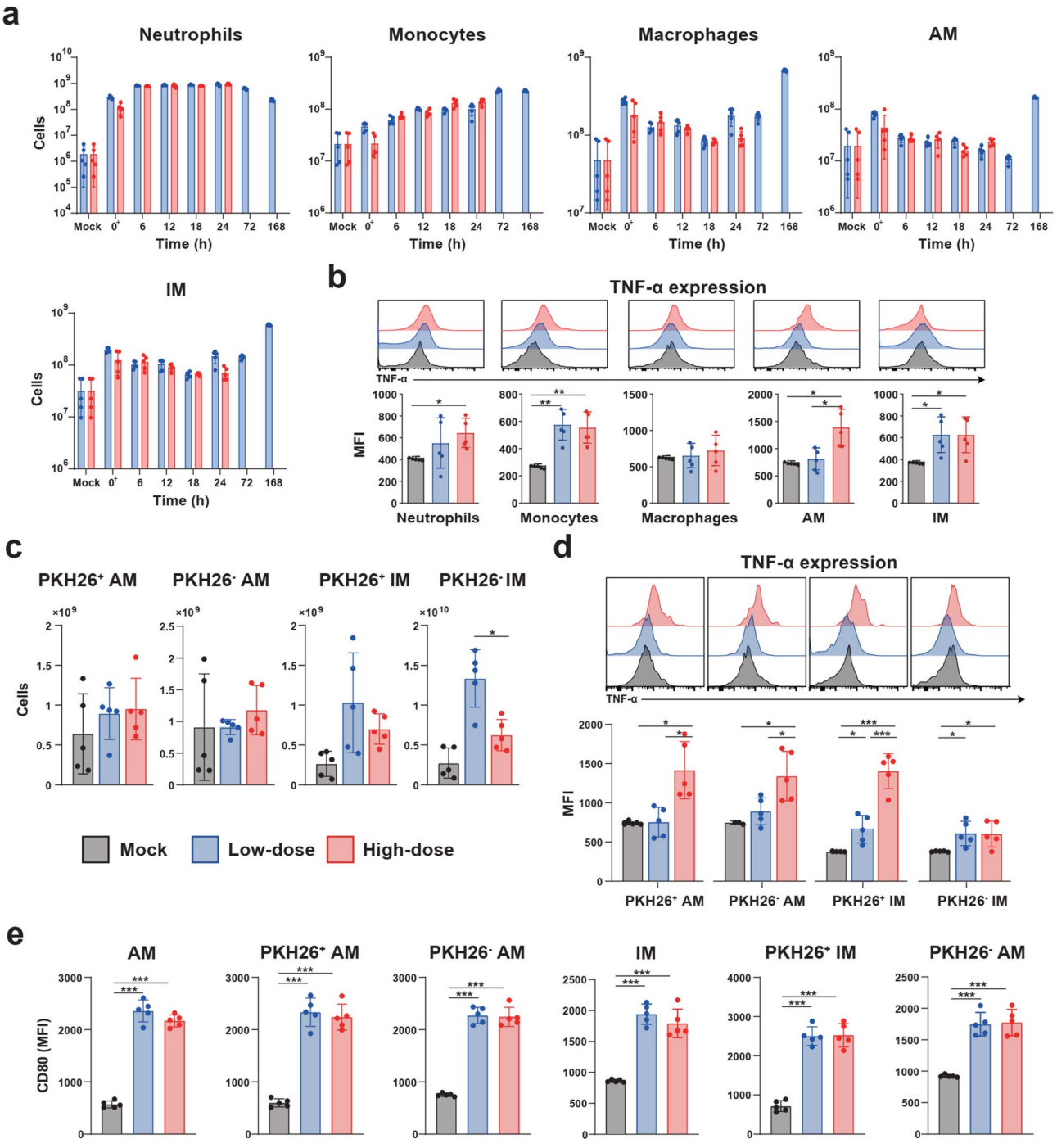

Fig. 3 Innate immune cell response during infection. **a**, Neutrophils, monocytes, macrophages, AM and IM changes before and after infection for high-dose and low-dose groups. **b**, TNF-α expression in neutrophils, monocytes, macrophages, AM and IM at 24 h post-infection. **c**, the ratio of PKH26$^+$ and PKH26$^-$ macrophages changed at 24 h post-infection. **d**, TNF-α expression in PKH26$^+$ and PKH26$^-$ macrophages at 24 h post-infection. **e**, CD80 expression in PKH26$^+$ and PKH26$^-$ macrophages at 24 h post-infection. AM, alveolar macrophage. IM, interstitial macrophage. *: $P < 0.05$, **: $P < 0.01$, ***: $P < 0.001$

KEGG analysis of up-regulated DEGs further validated the activation of these signal pathways, including TNF signaling pathway, IL-17 signaling pathway, C-type lectin receptor signaling pathway, RIG-like receptor signaling pathway, NOD-like receptor signaling pathway, TLR signaling pathway, chemokine signaling pathway, NFκB signaling pathway (Fig. 4e). Furthermore, KEGG analysis identified HIF-1 signaling pathway. The GO and KEGG analyses of down-regulated DEGs, as depicted in Figure S4ab, revealed associations with muscle contraction, circulation, and other related biological processes.

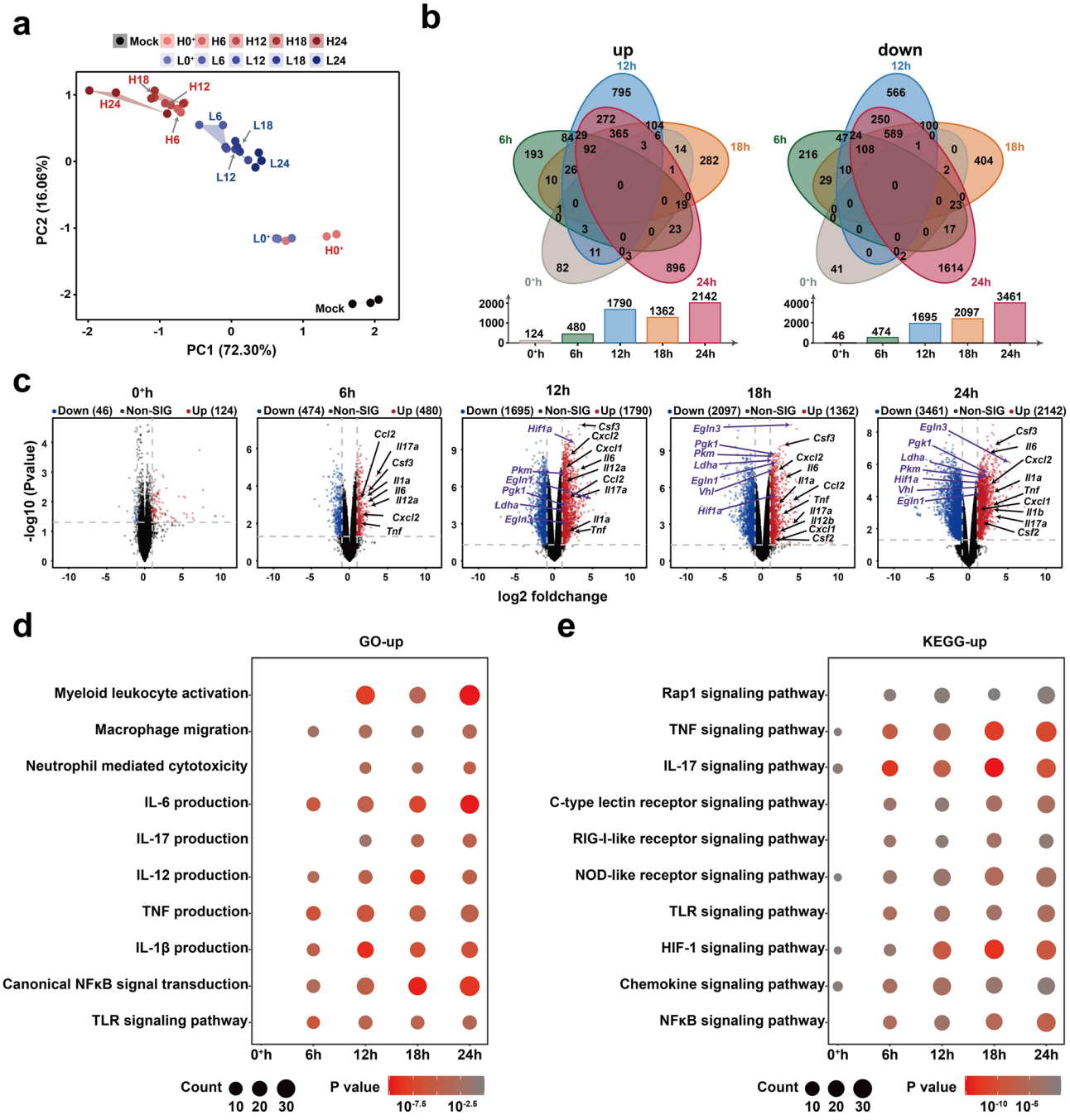

Fig. 4 Host RNA-seq analysis following *K. pneumoniae* infection. **a**, Principal component analysis results of RNA-seq data, with the same color representing replicate samples from the same time point and group. **b**, Venn diagram of upregulated and downregulated DEGs. **c**, Volcano plot of RNA-Seq transcriptome data, with significant DEGs highlighted in red (upregulated) or blue (downregulated). Genes denoted in dark font represent pro-inflammatory cytokines or chemokines, while those in violet indicate hypoxia-related genes. **d**, GO enrichment analysis of upregulated genes. **e**, KEGG enrichment analysis of upregulated genes. DEG, differentially expressed genes

However, these analyses did not identify any significant connections to immune system processes.

Due to the significant biological implications of upregulated DEGs, we categorized these DEGs into six gene clusters based on their expression patterns using Mfuzz. The number of genes in clusters 1–6 are 914, 644, 555, 430, 824, and 387, respectively (Fig. 5a). We found that clusters 1–4 have substantial biological significance, as there is at least one time point where the expression levels in the high-dose group are higher than those in the low-dose group. Subsequently, we utilized GO and KEGG enrichment analyses and discovered that the

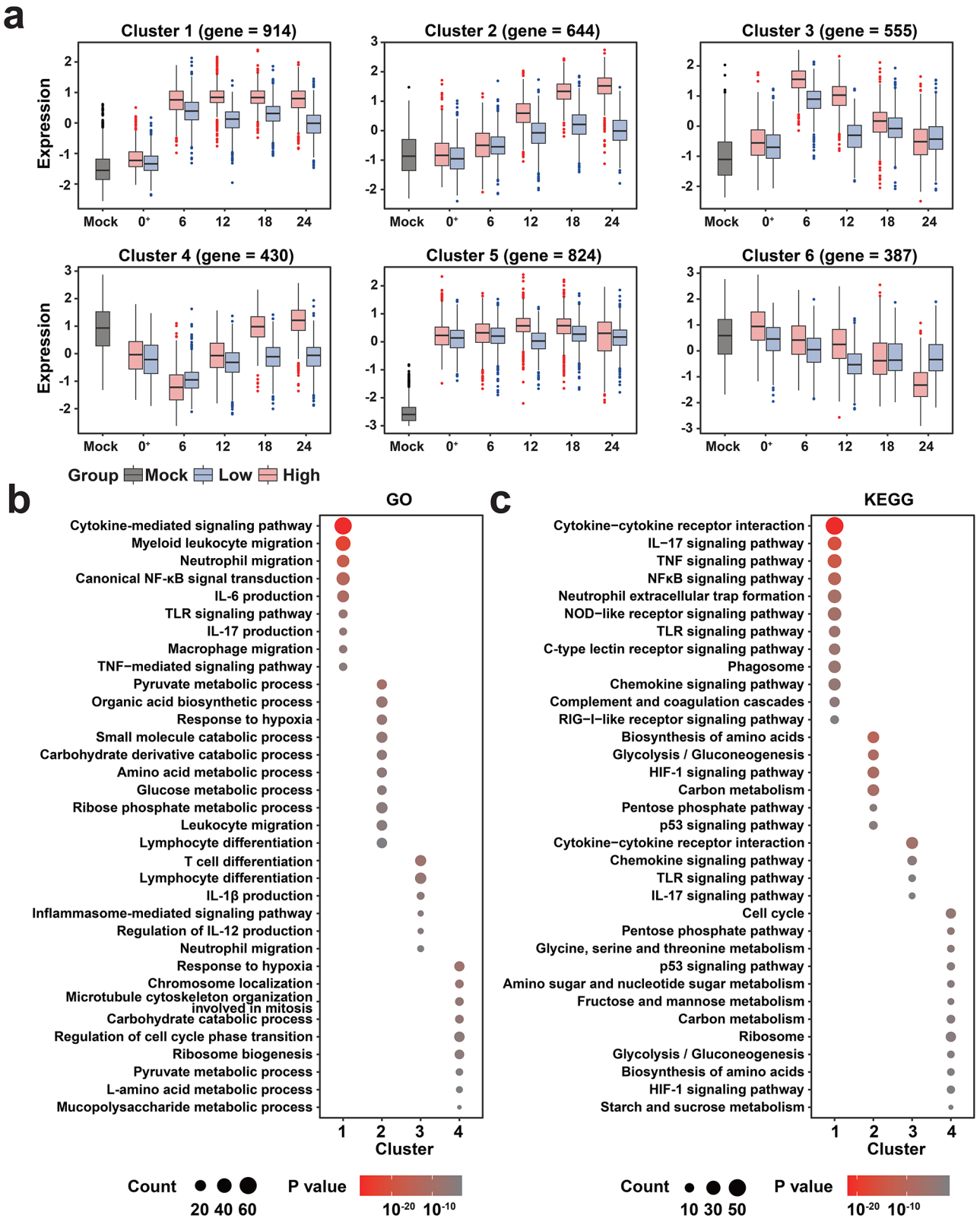

Fig. 5 Cluster analysis of up-regulated DEGs and their biological functions. **a**, Six distinct temporal gene expression patterns determined by Mfuzz clustering analysis. **b**, GO enrichment analysis for clusters 1 to 4. **c**, KEGG enrichment analysis for clusters 1 to 4

biological functions of clusters 1 and 3 are quite similar, both being associated with immune responses such as cytokines production, and phagocytes migration. Interestingly, GO analysis revealed that clusters 2 and 4 are associated with energy metabolism and hypoxia, as they are linked to several biological processes such as glucose metabolic process, carbohydrate derivative catabolic process, and response to hypoxia (Fig. 5b). KEGG analysis further supported these findings, showing that clusters 2 and 4 include pathways such as glycolysis/gluconeogenesis, carbon metabolism, and the HIF-1 signaling pathway (Fig. 5c).

K. pneumoniae significantly up-regulates siderophore-related genes to facilitate host invasion

In the lung tissues of each animal, we simultaneously conducted transcriptome analysis of bacteria. The PCA analysis of the *K. pneumoniae* transcripts revealed a very clear separation among groups (Fig. 6a). Considering that *K. pneumoniae* utilizes a variety of virulence factors for survival and pathogenesis, we focused our subsequent analyses on gene expression of virulence factors. The main studied virulence factors included lipopolysaccharide (LPS), capsule, adhesion, siderophores, metabolism, cell surface, lipid synthesis, protein synthesis, related to nucleic acid, transporters, regulators, and predicted virulence factors (Table S3) [22, 23]. Differential expression analysis was performed using the edgeR package to identify up-regulated and down-regulated genes (Figure S5). We found that only 62 virulence factors were expressed in NY13307, among which 20 virulence factors, mainly siderophore-related genes, were significantly up-regulated in high-dose group when compared to low-dose group during infection. By heatmap analysis, we observed that the expression of these 20 virulence factors was relatively low when the bacteria were in vitro, but in vivo, the expression levels in the high-dose group were higher than those in the low-dose group (Fig. 6b). GO enrichment analysis of the up-regulated DEGs revealed that the primary biological functions of the bacteria were related to siderophore biosynthetic process, siderophore metabolic process, and siderophore transport (Fig. 6c). Additionally, we conducted correlation analysis to study the relationship between the 20 virulence factor genes and the 6 clusters of genes in mice (from Fig. 5), and found that the correlation coefficients of cluster 1–6 were 0.730 ± 0.075, 0.576 ± 0.077, 0.507 ± 0.056, 0.161 ± 0.069, 0.436 ± 0.032, and 0.113 ± 0.073, respectively (Fig. 6d), indicating that these virulence factors are closely associated with inflammation and hypoxia of the host. According to the aforementioned results, the underlying mechanism by which high-dose *K. pneumoniae* leads to host death was summarized in Fig. 6e. We speculated that after challenge, high-dose bacteria secrete high levels of siderophores, leading to the secretion of large amounts of pro-inflammatory cytokines by host macrophages (AM and resident IM). Concurrently, the excessive secretion of siderophores triggers the activation of hypoxia signaling pathways. The interplay of these two phenomena may ultimately culminate in the death of the host.

Discussion

The present study demonstrated that MDR-KP NY13307 was selected through rigorous experimental screening from 18 clinical isolates, and an animal model of pneumonia infection was established via aerosolized intratracheal inoculation. High-dose bacteria led to severe pulmonary pathological changes, continuously increased bacterial load, significantly elevated secretion of inflammatory cytokines, and immune cell infiltration, when compared with low-dose bacteria. It was found that AM and resident IM were the primary cells secreting these cytokines. Further RNA-seq analysis revealed that hypoxia and pro-inflammatory cytokines were closely related to the survival of mice; the excessive secretion of siderophore in the high-dose group may be a key factor contributing to mortality.

Infections caused by MDR-KP have been associated with mortality rates exceeding 40–50% in critically ill patients and solid organ transplant recipients. In addition to adequate antibiotic treatment, there are currently no effective alternative therapies [24, 25]. Thus, there is an urgent need to investigate the pathogenesis of MDR-KP-induced mortality in mice. In our animal model, compared to the high-dose group, the low-dose group showed improvements in pathological changes, bacterial load, secretion of pro-inflammatory cytokines, and overall survival within 24 h post-infection (Figs. 1 and 2). Based on the results of cytokine secretion, we found that TNF-α showed differences between the two groups at the most time points (Fig. 2), prompting us to explore its cellular sources. Interestingly, there were no differences between the high-dose and low-dose groups in the trends of phagocytes, including neutrophils, monocytes, macrophages, AM, and IM, as well as the polarization of macrophages (Fig. 3).

The comparable immune cell recruitment between the two doses may stem from both activating a threshold in phagocyte mobilization, such that exceeding this threshold leads to a plateau in recruitment. AM are the first-line defenders of the alveoli and airways, while IM act as gatekeepers of the vasculature and lung interstitium, thus AM are the first to interact with bacteria. When their phagocytic function is overwhelmed, AM initiate inflammation by producing chemokines and cytokines (such as TNF-α and IL-1β) that recruit and activate neutrophils, monocytes, and dendritic cells [26], which is consistent with our experimental findings (Fig. 3b). IM are thought

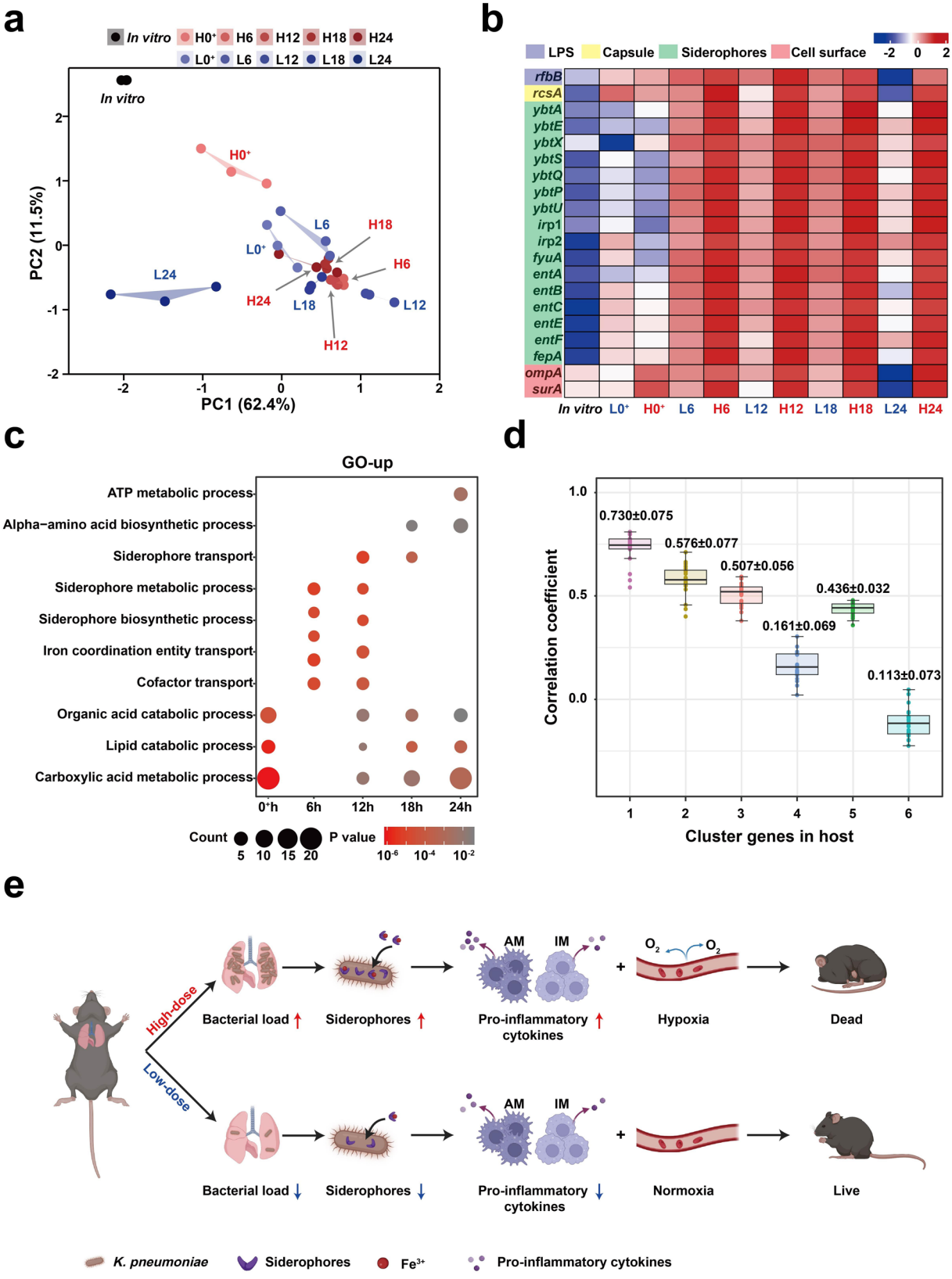

Fig. 6 Pathogen RNA-seq analysis following *K. pneumoniae* infection. **a**, Principal component analysis results of RNA-seq data, with the same color representing replicate samples from the same time point and group. **b**, Heatmap of 20 virulence factors. **c**, GO enrichment analysis of upregulated genes. **d**, Correlation analysis of 20 virulence factors in *K. pneumoniae* and 6 cluster genes in host. **e**, Putative pathogenesis of *K. pneumoniae* in mice

to be maintained or expanded by the recruitment of CCR2-dependent Ly6C + classical blood monocytes, at least in part. Following exposure to *K. pneumoniae*, splenic Ly6C + monocytes contribute significantly to the expansion of the IM pool endowed with enhanced immunoregulatory properties and are transformed into resident IM by staining with PHK26 dye [22]. Thus, we found that resident IM are secreting the pro-inflammatory cytokine TNF-α at 24 h post-infection (Fig. 3d). However, whether the effects of AM, resident IM, and TNF-α are beneficial or detrimental in this model requires further experimental validation.

On the host side, we have identified genes related to hypoxia that may be associated with survival outcomes. In diseases such as cystic fibrosis, chronic obstructive pulmonary disease, and bacterial infections, invading pathogens cause persistent inflammation in the lungs. The inflamed mucosa contains infiltrating neutrophils, as well as increased numbers of macrophages and dendritic cells. The alveolar space becomes poorly oxygenated or hypoxic, due to the accumulation of mucus and pus [27]. Previous study reported that hypoxia and bacterial infections often coexist in both acute and chronic clinical settings, and increased mortality is observed following systemic infection with *Streptococcus pneumoniae* in the setting of acute hypoxia [28]. Furthermore, the presence of hypoxia leads to the activation of hypoxia-inducible factors, which can contribute to innate immunity and inflammation through the expression of genes involved in the regulation of innate immunity and infection [27]. Hypoxia-inducible factors, particularly HIF-1α, sense hypoxia to regulate the expression of a series of downstream genes, which participate in multiple processes, including cell metabolism, cell growth/death, and so on. HIF-1α (*Hif1a*) proteins contain an oxygen-dependent degradation domain with two proline sites that are hydroxylated by the oxygen-dependent proline hydroxylase family, including PHD1 (*Egln2*), PHD2 (*Egln1*), and PHD3. Under hypoxia conditions, HIF-1α influences cell metabolism through two aspects [29]. On one hand, HIF-1α stimulates PGK (*Pgk1*) and LDHA (*Ldha*) to regulate the glycolysis process. On the other hand, HIF-1α induces anaerobic metabolism through multiple enzymes related to glycolysis and glucose transporters, such as pyruvate kinase M (*Pkm*), thereby producing energy. Thus, in this study, we observed that seven hypoxia-related genes, including *Hif1a*, *Egln1*, *Egln3*, *Vhl*, *Pgk1*, *Pkm*, and *Ldha*, were all up-regulated after 12 h post-infection (Fig. 4c) and the up-regulation of the glucose metabolic process and carbohydrate catabolic process (Fig. 5b,c), highlighting the consequence of inflammation and hypoxia.

On the pathogen side, LPS, capsule, siderophores, and cell surface related genes were significantly up-regulated during infection, with siderophores being particularly noteworthy. Iron is a scarce yet essential resource for *K. pneumoniae*, which must be obtained from the host to proliferate during infection. *K. pneumoniae* acquires iron through the secretion of siderophores that have a higher affinity for iron than host transport proteins. Siderophores can effectively sequester iron from host iron-chelating proteins [23]. Two types of siderophores are expressed in NY13307 and have been identified as up-regulated DEGs: enterobactin (*entA*, *entB*, *entC*, *entE*, *entF*, *fepA*) and yersiniabactin (*ybtA*, *ybtE*, *ybtX*, *ybtS*, *ybtQ*, *ybtP*, *ybtU*, *irp1*, *irp2*, *fyuA*) (Fig. 6b). Enterobactin is almost ubiquitous present among *K. pneumoniae* strains and is regarded as the primary iron uptake system [30]. In *K. pneumoniae*, the genes necessary for enterobactin biosynthesis are located on the chromosome within the *entABCDEF* gene cluster, while the *fepABCDG* gene cluster encodes the proteins responsible for its transport, with *fepA* specifically encoding the uptake receptor [31]. Importantly, *fepA* expression has been shown to be up-regulated during *K. pneumoniae* infection, indicating an enhancement of enterobactin functionality. Alongside enterobactin, yersiniabactin is overrepresented in *K. pneumoniae* isolates from the respiratory tract [32]. Notably, yersiniabactin is expressed during lung infection, and its activity remains uninhibited by lipocalin-2 (a host-secreted molecule that neutralizes enterobactin) in vivo during the early stages of lung infection. This is likely due to its significantly different structure from enterobactin, enabling *K. pneumoniae* to achieve high bacterial loads in the lungs during infection [32]. Therefore, these two types of siderophores may contribute to the proliferation and dissemination of *K. pneumoniae* in the high-dose group during infection. Previous studies also have shown that siderophore production is modulated by quorum sensing (QS) [33], a regulatory mechanism that relies on bacterial density. In our study, high-dose infections resulted in a more rapid increase in bacterial density compared to low-dose infections (Fig. 1d), likely enabling earlier QS activation and sustained high-density conditions. Once the bacterial population reaches a QS threshold, siderophore-related genes are upregulated to boost iron scavenging, a process that appears to be maintained in the high-dose group because of its continuously increasing bacterial load. Although we did not measure siderophore concentrations directly, dual RNA-seq data demonstrated a robust upregulation of both enterobactin and yersiniabactin gene clusters, which aligns with the proposed QS-mediated iron acquisition cascade. Future studies should validate this hypothesis by directly quantifying siderophore concentrations. This interplay among bacterial density, QS signaling, and siderophore biosynthesis likely facilitated the proliferation and dissemination of *K. pneumoniae* in

high-dose infections, highlighting the pathogen's adaptive strategies for exploiting host resources.

The secretion of siderophores may be closely correlated with the activation of the hypoxia signaling pathway and the release of pro-inflammatory cytokines, as indicated by the correlation analysis presented in Fig. 6d. This correlation suggests that siderophores may disrupt host iron homeostasis, leading to hypoxia and inflammation. Bacterial siderophores, such as enterobactin, sequester host iron with ultrahigh affinity, inducing intracellular iron deprivation. This iron scarcity inhibits prolyl hydroxylases (PHDs), stabilizing HIF-1α and activating hypoxia-responsive genes alongside proinflammatory cytokines. Holden et al. demonstrated that enterobactin evades the host iron-binding protein lipocalin-2, triggering HIF-1α stabilization and cytokine secretion in respiratory epithelial cells [34]. Holden et al. further showed that *K. pneumoniae* siderophores are essential for HIF-1α accumulation and lethal inflammation in murine pneumonia, as siderophore-deficient mutants failed to induce hypoxia or inflammation [35]. Complementing these findings, Wang et al. revealed that siderophores induce mitophagy-dependent apoptosis in platelets by disrupting mitochondrial iron-sulfur clusters, which generates ROS [36]. This ROS surge not only activates mitochondrial phagocytosis but also inhibits PHD activity through oxidative stress, creating a feedforward loop that amplifies HIF-1α stabilization and hypoxia signaling. Together, these studies provide a mechanistic framework wherein siderophores, whether through direct iron scavenging or ROS generation, converge on HIF-1α stabilization, supporting our hypothesis that bacterial iron acquisition strategies exacerbate hypoxia signaling and inflammatory pathology. Nevertheless, the specific mechanisms linking siderophores to hypoxia signaling require further validation. For instance, future studies using siderophore-deficient mutants could clarify whether HIF-1α stabilization and cytokine release depend on siderophore activity. Resolving these scientific questions would greatly facilitate the development of novel anti-infection interventions and the development of new vaccines, thereby making a significant contribution to the prevention and control of MDR-KP infections.

Conclusion

This study screened a strain of MDR-KP NY13307 from 18 clinical isolates and successfully established a corresponding mouse model of pneumonia infection using aerosolized intratracheal inoculation. High-dose bacterial exposure resulted in severe pulmonary pathological alterations, a continuous increase in bacterial load, significantly elevated secretion of inflammatory cytokines, and pronounced immune cell infiltration, compared to that of low-dose bacteria. AM and IM were predominantly responsible for the secretion of these cytokines. Based on further RNA-seq sequencing analysis, the overproduction of bacterial siderophores in the high-dose group may trigger hypoxia and the release of pro-inflammatory cytokines, ultimately leading to host mortality. However, the specific mechanisms underlying this process require further experimental validation.

Supplementary Information

The online version contains supplementary material available at https://doi.org/10.1186/s12866-025-04044-x.

Supplementary Material 1

Acknowledgements

Not applicable.

Author contributions

C. D., W. Y., Y. J., and D. Z. designed the study, supervised the whole project and revised the manuscript. X. S., C. S., and M. L. performed the experiments and bioinformatic analysis. X. S. was a major contributor in writing the manuscript. C. J. and C. D. performed statistical analysis. L. H. participated in the experimental performance and revised the manuscript. All authors read and approved the final manuscript.

Funding

This work is financially supported by the National Natural Science Foundation of China (Grant No. 12301644), and the Foundation of State Key Laboratory of Pathogen and Biosecurity of China (Grant No. SKLPBS2225).

Data availability

All data are available in the main text or the supplementary materials. The RNA-seq datasets used and/or analyzed during the current study have been deposited in the NCBI Gene Expression Omnibus (GEO) repository under accession number GSE289556.

Declarations

Ethics approval and consent to participate

All animal experiment protocols were reviewed and approved by Institutional Animal Care and Use Committee of Academy of Military Medical Sciences (Permit number: IACUC-DWZX-2024-007). Clinical trial number: not applicable.

Consent for publication

Not applicable.

Competing interests

The authors declare no competing interests.

Author details

[1]State Key Laboratory of Pathogen and Biosecurity, Academy of Military Medical Sciences, Beijing 100071, China
[2]Department of Mathematics, College of Basic Medicine, Army Medical University, Chongqing 400038, China

Received: 15 January 2025 / Accepted: 14 May 2025
Published online: 24 July 2025

References

1. Dorman MJ, Short FL. Genome watch: Klebsiella pneumoniae: when a colonizer turns bad. Nat Rev Microbiol. 2017;15:384.
2. Asri NAM, Ahmad S, Mohamud R, Hanafi NM, Zaidi NFM, Irekeola AA, et al. Global prevalence of nosocomial multidrug-resistant klebsiella pneumoniae: A systematic review and meta-analysis. Antibiotics. 2021;10:1508.

3. Opoku-Temeng C, Malachowa N, Kobayashi SD, Deleo FR. Innate host defense against Klebsiella pneumoniae and the outlook for development of immunotherapies. J Innate Immun. 2022;14:167–181.
4. Lin XC, Li CL, Zhang SY, Yang XF, Jiang M. The global and regional prevalence of Hospital-Acquired Carbapenem-Resistant Klebsiella pneumoniae infection: A systematic review and Meta-analysis. Open Forum Infect Dis. 2024;11:ofad649.
5. Arato V, Raso MM, Gasperini G, Scorza FB, Micoli F. Prophylaxis and treatment against klebsiella pneumoniae: current insights on this emerging antimicrobial resistant global threat. Int J Mol Sci. 2021;22:4042.
6. Wong Fok Lung T, Charytonowicz D, Beaumont KG, Shah SS, Sridhar SH, Gorrie CL, et al. Klebsiella pneumoniae induces host metabolic stress that promotes tolerance to pulmonary infection. Cell Metab. 2022;34:761–774.e9.
7. Zheng X, Guo J, Cao C, Qin T, Zhao Y, Song X, et al. Time-Course transcriptome analysis of lungs from mice infected with hypervirulent Klebsiella pneumoniae via aerosolized intratracheal inoculation. Front Cell Infect Microbiol. 2022;12:8330801–15.
8. Mackel JJ, Mick CLG, Guo E, Rosen DA. Lung infection with classical Klebsiella pneumoniae strains establishes robust macrophage-dependent protection against heterologous reinfection. Microbes Infect. 2024;26:105369.
9. Westermann AJ, Gorski SA, Vogel J. Dual RNA-seq of pathogen and host. Nat Rev Microbiol. 2012;10:618–630.
10. Janssen AB, de Bakker V, Aprianto R, Trebosc V, Kemmer C, Pieren M, et al. Klebsiella pneumoniae OmpR facilitates lung infection through transcriptional regulation of key virulence factors. Microbiol Spectr. 2024;12:e03966231–17.
11. Song X, Zhang W, Zhai L, Guo J, Zhao Y, Zhang L, et al. Aerosolized intratracheal inoculation of Recombinant protective antigen (rPA) vaccine provides protection against inhalational Anthrax in B10.D2-Hc0 mice. Front Immunol. 2022;13:819089.
12. Yuan X, Song X, Zhang X, Hu L, Zhou D, Zhang J, et al. Unraveling host-pathogen dynamics in a murine model of septic peritonitis induced by vancomycin-resistant Enterococcus faecium. Virulence. 2024;15:2367659.
13. Robinson MD, McCarthy DJ, Smyth GK. EdgeR: A bioconductor package for differential expression analysis of digital gene expression data. Bioinformatics. 2010;26:139–140.
14. Yu G, Wang LG, Han Y, He QY, ClusterProfiler. An R package for comparing biological themes among gene clusters. Omi J Integr Biol. 2012;16:284–287.
15. Kumar L, Futschik ME, Mfuzz. A software package for soft clustering of microarray data. Bioinformation. 2007;2:5–7.
16. Chen J, Zhang H, Liao X. Hypervirulent Klebsiella pneumoniae. Infect Drug Resist. 2023;16:5243–5249.
17. Podschun R, Ullmann U. Klebsiella spp. As nosocomial pathogens: epidemiology, taxonomy, typing methods, and pathogenicity factors. Clin Microbiol Rev. 1998;11:589–603.
18. Wang LT, Yen BL, Wang HH, Chao YY, Lee W, Huang LY, et al. Placental mesenchymal stem cells boost M2 alveolar over M1 bone marrow macrophages via IL-1β in Klebsiella-mediated acute respiratory distress syndrome. Thorax. 2023;78:504–514.
19. Xiong H, Keith JW, Samilo DW, Carter RA, Leiner IM, Pamer EG. Innate Lymphocyte/Ly6Chi monocyte crosstalk promotes Klebsiella Pneumoniae clearance. Cell. 2016;165:679–689.
20. Lee IM, Huang TY, Yang FL, Johansson V, Hsu CR, Hsieh PF, et al. A hexasaccharide from capsular polysaccharide of carbapenem-resistant Klebsiella pneumoniae KN2 is a ligand of Toll-like receptor 4. Carbohydr Polym. 2022;278:118944.
21. Mancuso P, Curtis JL, Weitzel AM, Griffin CA, Bouchard B, Freeman CM, et al. Diet-induced obesity in mice impairs host defense against Klebsiella pneumonia in vivo and glucose transport and bactericidal functions in neutrophils in vitro. Am J Physiol - Lung Cell Mol Physiol. 2022;322:L116–L128.
22. Monteiro A, de Cordeiro SS, Reis SM. Virulence factors in Klebsiella pneumoniae: A literature review. Indian J Microbiol. 2024;64:389–401.
23. Paczosa MK, Mecsas J. Klebsiella pneumoniae: going on the offense with a strong defense. Microbiol Mol Biol Rev. 2016;80:629–661.
24. Xu L, Sun X, Ma X. Systematic review and meta-analysis of mortality of patients infected with carbapenem-resistant Klebsiella pneumoniae. Ann Clin Microbiol Antimicrob. 2017;16:18.
25. Tumbarello M, Trecarichi EM, De Rosa FG, Giannella M, Giacobbe DR, Bassetti M, et al. Infections caused by KPC-producing Klebsiella pneumoniae: differences in therapy and mortality in a multicentre study. J Antimicrob Chemother. 2015;70:2133–2143.
26. Aegerter H, Lambrecht BN, Jakubzick CV. Biology of lung macrophages in health and disease. Immunity. 2022;55:1564–15 80.
27. Schaible B, Schaffer K, Taylor CT. Hypoxia, innate immunity and infection in the lung. Respir Physiol Neurobiol. 2010;174:235–243.
28. Thompson AAR, Dickinson RS, Murphy F, Thomson JP, Marriott HM, Tavares A, et al. Hypoxia determines survival outcomes of bacterial infection through HIF-1α–dependent reprogramming of leukocyte metabolism. Sci Immunol. 2017;2:eaal2861.
29. Luo Z, Tian M, Yang G, Tan Q, Chen Y, Li G, et al. Hypoxia signaling in human health and diseases: implications and prospects for therapeutics. Signal Transduct Target Ther. 2022;7:218.
30. El Fertas-Aissani R, Messai Y, Alouache S, Bakour R. Virulence profiles and antibiotic susceptibility patterns of Klebsiella pneumoniae strains isolated from different clinical specimens. Pathol Biol. 2013;61:209–216.
31. Müller SI, Valdebenito M, Hantke K. Salmochelin, the long-overlooked catecholate siderophore of Salmonella. Biometals. 2009;22:691–695.
32. Bachman MA, Oyler JE, Burns SH, Caza M, Lépine F, Dozois CM, et al. Klebsiella pneumoniae Yersiniabactin promotes respiratory tract infection through evasion of Lipocalin 2. Infect Immun. 2011;79:3309–3316.
33. Ren D, Zuo R, Wood TK. Quorum-sensing antagonist (5Z)-4-bromo-5-(bromomethylene)-3-butyl-2(5H)- furanone influences siderophore biosynthesis in Pseudomonas putida and Pseudomonas aeruginosa. Appl Microbiol Biotechnol. 2005;66:689–695.
34. Holden VI, Lenio S, Kuick R, Ramakrishnan SK, Shah YM, Bachman MA. Bacterial siderophores that evade or overwhelm Lipocalin 2 induce hypoxia inducible factor 1α and Proinflammatory cytokine secretion in cultured respiratory epithelial cells. Infect Immun. 2014;82:3826–3836.
35. Holden VI, Breen P, Houle S, Dozois CM, Bachman MA. Klebsiella pneumoniae siderophores induce inflammation, bacterial dissemination, and HIF-1α stabilization during pneumonia. MBio. 2016;7.
36. Wang W, Lu Y, Wang Y, Zhang Y, Xia B, Cao J. Siderophores induce mitophagy-dependent apoptosis in platelets. Ann Transl Med. 2020;8:879.

Publisher's note

Springer Nature remains neutral with regard to jurisdictional claims in published maps and institutional affiliations.